Available online at www.sciencedirect.com
ScienceDirect
Catalysis Today 117 (2006) 133–137
CATALYSIS TODAY
www.elsevier.com/locate/cattod

Mechanism of methane oxidation by transition metal oxides: A cluster model study

Gang Fu, Xin Xu *, Huilin Wan *

State Key Laboratory of Physical Chemistry of Solid Surfaces & Center for Theoretical Chemistry, Department of Chemistry & Institute of Physical Chemistry, Xiamen University, Xiamen, China

Available online 18 July 2006

Abstract

We present a systematic survey of C–H activation over various transition metal oxides using cluster model calculations. We find that H abstraction pathway is feasible on most oxides. Our calculations suggest that when the M=O bond possesses a high polarity such as those in tungsten oxides, (2 + 2) becomes an alternative pathway. Trends and intrinsic factors that influence the activation modes are discussed.

Keywords: Methane oxidation; Transition metal oxide; C–H bond activation; H abstraction

1. Introduction

Lower alkanes are the main constituents of natural gas. While abundant in nature, there are limited industrial processes using these 'cheap' resources owing to the relative chemical inertness of a C–H bond and the difficulty to achieve the selective activation of a C–H bond. Developing efficient strategies for the selective oxidation of lower alkanes to value-added chemicals or liquid fuels has far-reaching significance. Especially, the direct conversion of methane to oxygenates such as CH_3OH and HCHO is viewed as one of the most challenging goals in catalysis [1–9].

Selective oxidation of methane to oxygenates was often carried out over supported transition metal oxides. Among various catalysts employed, V_2O_5 [10–12] and MoO_3 [1,13–15] were considered to be the most active and selective catalysts, while recent studies showed that Fe [16–18] and W [19,20] oxides are also of great promise. Moreover, McCormick et al. [21] reported a promoted effect of Cr addition, which increases the HCHO selectivity. However, a high temperature is generally required for the activation of methane, and at such temperature, the desired oxygenates would be quickly oxidized into unwanted carbon oxides. Therefore, in spite of great effort, the single-pass yield of oxygenates is still quite low, usually less than 4%, far from fulfilling the industrial requirement [7]. Thus, the questions on how to conquer the propensity of over-oxidation of CH_3OH and/or HCHO to CO_x, and how to develop an efficient catalytic system of both good activity and good selectivity call for a detailed mechanistic understanding.

Although a number of mechanistic works concerning the selective alkane oxidations were reported [22–30], much remains obscure for the molecular details of the activation mechanisms. For instance, what is the most favorable C–H bond activation pathway over a specific metal oxide? How is the reactivity connected with the redox and acid–base properties of the oxide catalysts? How does the reactivity change for metal oxides across the row and down the column of the periodic table? In the previous work, we have investigated methane [31] and propane [32] activation on molybdenum oxide model catalyst. We found that H abstraction by the terminal oxygen is the most feasible reaction pathway, which can account for most of the experimental observations. Here, we extend our study to vanadium, chromium and tungsten oxides, and compare the results to those of the molybdenum oxide, trying to explore the controlling factors that govern the various reaction pathways.

2. Model of choice and computational methods

We choose M_3O_9 (M = Cr, Mo and W) and $V_3O_6Cl_3$ clusters as model catalysts (Fig. 1). This kind of M_3O_9 cluster models

* Corresponding author. Tel.: +86 592 2182219; fax: +86 592 2183047.
E-mail addresses: xinxu@xmu.edu.cn (X. Xu), hlwan@xmu.edu.cn (H. Wan).

0920-5861/$ – see front matter © 2006 Published by Elsevier B.V.
doi:10.1016/j.cattod.2006.05.048

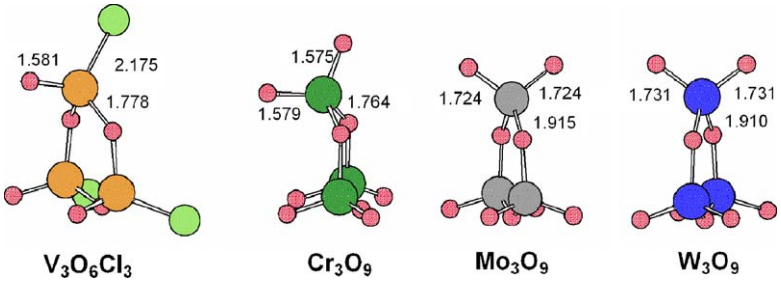

Fig. 1. $V_3O_6Cl_3$ and M_3O_9 (M = Cr, Mo, W) cluster models, which provides various kinds of terminal [=O] and bridge [–O–] active sites such as M=O, O=M=O, M–O–M, O=M–O–Mo=O, etc. Keys—yellow circle: V; green circle: Cr; grey circle: Mo; blue circle: W; red circle: O, light green circle: Cl. (For interpretation of the references to color in this figure legend, the reader is referred to the web version of this article.)

has been successfully applied before in the study of alkanes activation on the molybdenum oxide [31–33]. Experimentally, it is well known that the oxide cluster itself can serve as an active oxidant in both solution and gas phase [33–36], and there are many experimental implications that 2d oligomeric oxide domains formed on the supported catalysts which represented a good selective oxidation performance [18,37–40].

We concentrated on the activation of C–H bonds by terminal oxygens [=O] and bridge oxygens [–O–]. We considered eight possible mechanisms. We referred to **T1** and **T2** as the (2 + 2) additions (Fig. 2), which lead to the carbide and the hydride formation, respectively. As the valence of the metal center is not changed during the reaction, (2 + 2) might be considered as an acid–base reaction. **T3**–**T5** belong to a two-electron (2e) oxidation process with the metal center being reduced formally by two units (Fig. 3). **T3** and **T4** correspond to the (3 + 2) and (5 + 2) pathways, respectively. Both of them lead to the formation of hydroxyl and alkoxy directly. **T5** is called the oxenoid insertion, which leads directly to the formation of alcohol. H abstraction is a 1e process (Fig. 4), which involves radical formation with the metal center being reduced formally by one unit. Here we considered H abstractions both by terminal oxygens (**T6** and **T7**) and bridge oxygens (**T8**).

The quantum calculations were performed using hybrid density functional theory at the level of B3LYP [41,42]. Full geometry optimizations and analytical frequency calculations were performed with basis sets of double zeta quality (6-31G [43]) for the main group elements. The final energies were calculated with polarization functions being included (6-31G** [44]). Hay's effective core potentials (Lanl2dz [45] denoted in Gaussian 98 [46]) were used for transition metals, which include the relativistic effects for heavy metals. The methodology used here was shown to lead to satisfactory results as compared to the higher level calculations and the related experimental data [31,32]. Energy barriers reported here are after zero-point energy corrections and thermo corrections to 873 K, which corresponds to the experimental condition [7].

3. Results and discussion

Fig. 2 depicted the transition states of **T1** and **T2**. Either **T1** or **T2** occurs via a four-center, four-electron cyclic structure. Although both **T1** and **T2** belong to the (2 + 2) addition, we find that **T1** is significantly favored over **T2** by about 30 kcal/mol. Such a tendency may be explained by the dipole interaction. In fact, the initial orientation of the $C^{\delta-}$–$H^{\delta+}$ bond polarity in **T2** is opposed to that of the $M^{\delta+}$–$O^{\delta-}$ bond, destabilizing the transition state [47]. Previous calculations showed that the positive charge on the metal center increases from Cr to Mo to W [47]. Thus, the M–O bond polarity increases down the column or to the left of the row in accordance with the periodic trend of electronegativity. The calculated barriers for **T1** are 57.0 kcal/mol (V), 50.1 kcal/mol (Mo) and 43.6 kcal/mol (W). Although we are unable to locate a **T1** state for Cr, we expect it to be substantially higher than that of V. Thus, for **T1**, we

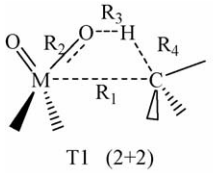

T1 (2+2)

M	R_1	R_2	R_3	R_4	ΔE_a
V	2.366	1.677	1.160	1.601	57.0
Cr	-	-	-	-	-
Mo	2.419	1.833	1.214	1.493	50.1
W	2.365	1.827	1.254	1.467	43.6

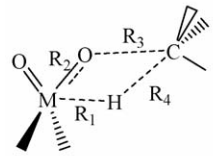

T2 (2+2)

M	R_1	R_2	R_3	R_4	ΔE_a
V	1.621	1.631	2.116	1.971	86.5
Cr	1.575	1.645	2.051	1.848	82.5
Mo	1.752	1.791	2.133	1.998	86.9
W	1.767	1.790	2.170	1.995	78.9

Fig. 2. Schematic representation of transition states **T1** and **T2**. These are the (2 + 2) additions, leading to the carbide and the hydride formation, respectively. Geometric parameters and barrier heights are labelled, which vary as M in metal oxides MO_x change periodically.

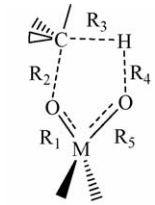

M	R_1	R_2	R_3	R_4	R_5	ΔE_a
V	-	-	-	-	-	-
Cr	1.621	2.254	1.592	1.098	1.685	42.8
Mo	1.783	2.077	1.790	1.054	1.853	68.6
W	1.800	2.033	1.837	1.041	1.865	83.8

T3 (3+2)

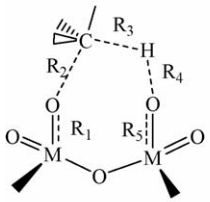

M	R_1	R_2	R_3	R_4	R_5	ΔE_a
V	1.619	2.342	1.853	1.038	1.719	63.6
Cr	1.614	2.475	1.687	1.049	1.714	39.7
Mo	1.771	2.300	1.751	1.057	1.855	63.2
W	1.777	2.252	1.869	1.402	1.849	80.2

T4 (5+2)

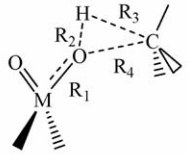

M	R_1	R_2	R_3	R_4	ΔE_a
V	1.727	0.975	2.130	2.583	69.4
Cr	1.766	1.034	1.606	2.289	39.2
Mo	1.918	0.995	1.895	2.314	69.4
W	1.902	0.980	2.037	2.347	87.3

T5 oxenoid insertion

Fig. 3. Schematic representation of transition states **T3–T5**. These are the two-electron oxidation processes of C–H. While **T3** and **T4** correspond to the (3 + 2) and (5 + 2) pathways, respectively, leading to the formation of hydroxyl and alkoxy directly; **T5** is the oxenoid insertion, which leads directly to the formation of alcohol. Geometric parameters and barrier heights are labelled, which vary as M in metal oxides MO_x change periodically.

conclude the reactivity follows the trend W > Mo > V > Cr, in parallel with the polarity of an M–O bond.

Since the (2 + 2) addition eventually involves the breakage of the M=O π bond, the π bond strength is another factor that enters the reactivity of metal oxides. Previous calculations showed that the π bond becomes stronger for the heavier metal [48]. Hence, a stronger M=O π bond is correlated with a lower reactivity of the metal oxide. For **T2**, we observe an abnormal

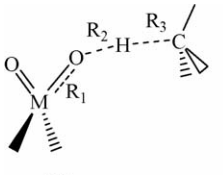

M	R_1	R_2	R_3	ΔE_a
V	1.695	1.170	1.397	35.5
Cr	1.691	1.199	1.333	20.1
Mo	1.841	1.068	1.578	45.0
W	1.824	1.058	1.606	56.8

T6

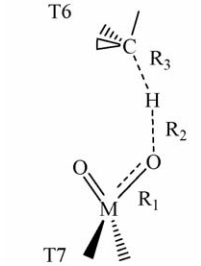

M	R_1	R_2	R_3	ΔE_a
V	1.703	1.134	1.439	36.8
Cr	1.715	1.279	1.277	24.2
Mo	1.850	1.155	1.429	49.7
W	1.838	1.126	1.485	59.6

T7

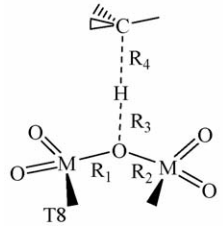

M	R_1	R_2	R_3	R_4	ΔE_a
V	1.928	1.837	1.230	1.340	42.7
Cr	1.886	1.831	1.266	1.297	33.1
Mo	2.045	2.045	1.088	1.580	63.6
W	2.109	2.001	1.081	1.607	79.3

T8

Fig. 4. Schematic representation of transition states **T6–T8**. These are the H abstraction processes, involving one-electron oxidations of C–H. While **T6** and **T7** use terminal oxygens in anti and syn modes, respectively, **T8** use bridge oxygens. Geometric parameters and barrier heights are labelled, which vary as M in metal oxides MO_x change periodically.

trend for reactivity in that W > Cr > V > Mo. This can be rationalized by the competition between two opposing factors—the π bond strength and the polarity of M–O.

Geometric parameters reveal some other mechanistic details (Fig. 2). For **T1**, the R_3 distance (O···H) decreases from W (1.254 Å) to Mo (1.214 Å) to V (1.160 Å); which accompanies the increase of the R_4 distance (C···H) from W (1.467 Å) to Mo (1.493 Å) to V (1.601 Å). Thus, we expect that **T1** state for Cr is even late with a short O···H bond and a long C···H distance, whereas an early transition state is preferred for the **T1** pathway. As compared to **T1**, **T2** would always be considered as a late transition state in that the M–H bond (1.6–1.8 Å) is already formed and the C–H bond (1.8–2.0 Å) is broken. Note that, however, the formation of the O···C bond is still at its early stage (2.1 Å versus 1.43 Å of an ordinary C–O single bond).

In pathways from **T3** to **T5** (Fig. 3), the metal centers are reduced by two units. Thus, the reactivity should be correlated with the trend of reducibility of metal oxides. For the singlet electronic state of the M_3O_9 model, it is expected that the lowest unoccupied molecular orbital (LUMO) is made from the M=O π* anti-bonding. Hence, a stronger M=O π bond is correlated with a higher lying LUMO, in accordant connection with a lower reducibility of the metal oxide. We therefore expect that the reactivity decreases down the column or to the left of the row as the M=O π bond strength increases [47].

For **T4**, the calculated barriers are 63.6 kcal/mol (V), 39.7 kcal/mol (Cr), 63.2 kcal/mol (Mo) and 80.2 kcal/mol (W). Thus, the reactivity is Cr > Mo ≈ V > W. For **T3**, the calculated barriers are 42.8 kcal/mol (Cr), 68.6 kcal/mol (Mo) and 83.8 kcal/mol (W), suggesting the same trend as Cr > Mo > W. Note that **T4** is always preferable over the corresponding **T3**. This can be rationalized by the spectator oxo effect such that the relaxation effect is more significant in **T4** than that in **T3** [48]. As the oxenoid insertion (**T5**) is proposed to prefer for the electrophilic oxygen species, the reactivity of **T5** should also coincide with the basicity of the oxygens. Therefore, the reactivity decreases as the oxygen in M=O becomes more negative charged with M varies down the column or to the left of the row [47]. The calculated barriers for **T5** are 69.4 kcal/mol (V), 39.2 kcal/mol (Cr), 69.4 kcal/mol (Mo) and 87.3 kcal/mol (W), again leading to the same trend of Cr > Mo ≈ V > W as in **T3** and **T4**.

Geometrically (Fig. 3), we see that in **T5**, the R_1 distance is fully elongated from the M=O double bond to the M–O single bond, while the O–H bond (R_2) is fully formed. As **T5** will eventually lead to the direct formation of alcohol, we expect the barriers are best correlated with the R_3 (C···H) and R_4 (C···O) distances. Indeed we see that R_3 and R_4 increase from Cr to Mo to W down the column or to V to the left of the row, in good agreement with the increased tendency of ΔE_a.

In **T3** and **T4**, we see that the O···H bond ($R_4 \approx 1.0$ Å) is almost formed, whereas the O···C formation is still at the early stage ($R_2 \approx 2.0$ Å). We find that the calculated barrier heights are best correlated with the breaking C···H bond (R_3) such that an early transition state with a short R_3 is related to a small ΔE_a.

In line with other theoretical works [24], our pervious work [31] suggested that (5 + 2) may become an important pathway when there are terminal oxygens within the suitable distance. For all the model catalysts examined here, the [=O]···[O=] distance are found to vary from 3.81 to 5.36 Å. Nevertheless, except Cr, where **T3**–**T5** are more favorable than **T1**, our present calculations reveal that all other metal oxides possess a higher barrier regardless of the [=O]···[O=] distance. This finding downplays the role of the (3 + 2) and (5 + 2) pathways on most oxide surfaces.

T6–**T8** are for H abstraction (Fig. 4), which are 1e processes, giving an MO–H bond and a methyl radical. We expect that the MO–H bond strength decreases as the metal varies down the periodic column and to the left of the periodic row, since the penalty to open the M=O π bond has to be paid upon forming the O–H bond such that the MO–H bond strength anti-parallels with the M=O π bond strength. Thus, we see that the reactivity follows the trend that Cr > V > Mo > W. It is no wonder that H abstractions by terminal [=O] are much more favored over that by bridge [–O–], as the later disturbs the M–O σ bond, which is stronger than the corresponding M–O π bond, upon forming the O–H bond.

Here we note that the 1e processes (**T6**–**T8**) are generally more favorable than those involving 2e oxidation of C–H (**T3**–**T5**); and the anti mode (**T6**) is superior to the corresponding syn mode (**T7**). Geometrically (Fig. 4), we may correlate the R_2 (O···H) and R_3 (C···H) distances with the barrier heights. Thus in **T6**, we see that R_2 decreases from 1.199 Å (Cr) to 1.068 Å (Mo) to 1.058 Å (W), while R_3 increases from 1.333 Å (Cr) to 1.578 Å (Mo) to 1.606 Å (W). This is accompanied by ΔE_a increased from 20.1 kcal/mol (Cr) to 45.0 kcal/mol (Mo) to 56.8 kcal/mol (W). Numbers for V are in between Cr and Mo. Hence, R_2 and R_3 are 1.170 and 1.397 Å with ΔE_a being 35.5 kcal/mol.

Among the eight pathways considered here, the most favorable pathway is anti-H abstraction (**T6**) by terminal oxygen with the exception of W_3O_9, where (2 + 2) (**T1**) appears to be the best pathway. In general, we find that H abstraction mechanism can account for most of the experimental observations:

(1) The calculated barriers are 35.5 kcal/mol for CH_4 activation on the V oxide and 45.0 kcal/mol on the Mo oxide [31], in good agreement with the experimental values (39.9 kcal/mol [12] and 45.2 kcal/mol [13] for V and Mo base oxides, respectively). We have also performed similar calculations for H abstraction from methylene group in propane by Mo_3O_9 [32] and $V_3O_6Cl_3$ [49]. The predicted activation enthalpies are 23.8 and 32.0 kcal/mol for V and Mo oxide, in compatible with experimental values of 23.7 and 28.0 kcal/mol measured on VO_x/ZrO_2 and MoO_x/ZrO_2, respectively [50]. The general agreement between theory and experiment lends support to the proposal that H abstraction is generally feasible for alkane activations.

(2) Recent EPR spectra [30] showed that when *n*-pentane flowed through the tungstated zirconia catalyst, W^{6+} centers were reduced to W^{5+} and organic radicals formed. This experimental observation is in line with the H abstraction pathway of a one-electron process. For methane activation over the W_3O_9 model catalyst, we find that the most favorable pathway is (2 + 2) (ΔE_a = 43.6 kcal/mol) rather

than H abstraction (ΔE_a = 56.8 kcal/mol). But when methane is replaced by pentane [51], the same level of calculations lead to ΔE_a = 43.5 kcal/mol for H abstraction as opposed to ΔE_a = 44.4 kcal/mol for (2 + 2).

4. Conclusions

We present a comprehensive survey of different C–H activation mechanisms over various transition metal oxide clusters by means of UB3LYP/6-31G**//UB3LYP/6-31G level of theory. Emphasis has been laid on how a reaction pathway is favored or disfavor as the metal center varies down the periodic column from Cr to Mo to W or to the left of the periodic row to V. The M–O bond polarity and the M=O π bond strength are two opposing factors. While (2 + 2) of the nature of acid–base reaction is mostly governed by the M–O bond polarity such that it is most favorable over the W oxide; the other pathways involve the reduction of the metal center such that the Cr oxide is the best candidate owing to its lowest the M=O π bond strength which is accompanied by the highest reducibility of the metal center. A fairly good compliance between H abstraction mechanism and experimental evidences supports that H abstraction is the working mechanism for the activation of alkanes on most high valence transition metal oxides. We also infer that the interplay between the M–O bond polarity and the M=O π bond strength may counterbalance the reactivity and the selectivity, hence V and Mo oxides are the most active and selective catalysts experimentally observed [1,10–15].

Acknowledgements

This work is supported by the Ministry of Science and Technology (2005CB221408, 2004CB719902), NSFC (20433030, 20525311, 20533030, 20021002, 20503022), TRAPOYT from the Ministry of Education and innovation project of Xiamen University (20041008).

References

[1] N.R. Foster, Appl. Catal. 85 (1985) 1.
[2] H.D. Gesser, N.R. Hunter, C.B. Prakash, Chem. Rev. 85 (1985) 235.
[3] G.A. Fould, B.F. Gray, Fuel Proc. Tech. 42 (1995) 129.
[4] T.J. Hall, J. Hargreaves, G.J. Huncthing, R.W. Richard, W. Joyner, S.H. Taylor, Fuel Proc. Tech. 42 (1995) 151.
[5] A.E. Shilov, G.B. Shul'pin, Chem. Rev. 97 (1997) 2879.
[6] R.H. Crabtree, J. Chem. Soc. Dalton Trans. (2001) 2437.
[7] K. Otsuka, Y. Wang, Appl. Catal. A 221 (2001) 145.
[8] K. Tabata, Y. Teng, T. Takemoto, E. Suzuki, M.A. Banares, M.A. Pena, J.L.G. Fierro, Catal. Rev. 44 (2002) 1.
[9] F. Arena, A. Parmaliana, Acc. Chem. Res. 36 (2003) 867.
[10] M.M. Khan, G.A. Somorjai, J. Catal. 91 (1985) 263.
[11] N.D. Spencer, C.J. Pereira, J. Catal. 116 (1989) 399.
[12] K.J. Zhen, M.M. Khan, C.J. Mak, K.B. Lewis, G.A. Somorjai, J. Catal. 94 (1985) 501.
[13] N.D. Spencer, C.J. Pereira, AIChE J. 33 (1987) 1808.
[14] M.R. Smith, U.S. Ozkan, J. Catal. 141 (1993) 124.
[15] X. Zhang, D.H. He, Q.J. Zhang, Q. Ye, B.Q. Xu, Q.M. Zhu, Appl. Catal. A 249 (2001) 107.
[16] T. Kobayashi, K. Nakagawa, K. Tabata, M. Haruta, J. Chem. Soc. Chem. Commun. (1994) 1609.
[17] Y. Wang, K. Osuka, J. Catal. 155 (1995) 256.
[18] F. Arena, G. Gatti, G. Martra, S. Coluccia, L. Stievano, L. Spadaro, P. Famulari, A. Parmaliana, J. Catal. 231 (2005) 365.
[19] A. de Lucas, J.L. Valverde, P. Canizares, Appl. Catal. A 172 (1998) 165.
[20] A. de Lucas, J.L. Valverde, P. Canizares, Appl. Catal. A 184 (1999) 143.
[21] R.L. McCormick, G.O. Alptekin, A.M. Herring, T.R. Ohno, S.F. Dec, J. Catal. 172 (1997) 160.
[22] (a) K. Yoshizawa, Y. Shiota, T. Yamabe, J. Am. Chem. Soc. 120 (1998) 564; (b) K. Yoshizawa, Y. Shiota, T. Yamabe, Organometallics 17 (1998) 2785; (c) K. Yoshizawa, Y. Shiota, T. Yumura, T. Yamabe, J. Phys. Chem. B 104 (2000) 734; (d) K. Yoshizawa, Coord. Chem. Rev. 226 (2002) 251, and reference therein.
[23] H.F. Liu, R.S. Liu, D.Y. Liew, R.E. Johnson, J.H. Lunsford, J. Am. Chem. Soc. 106 (1984) 4117.
[24] F. Gilardoni, A.T. Bell, A. Chakraborty, P. Boulet, J. Phys. Chem. B 104 (2000) 12250.
[25] B. Grzybowska-Swierkosz, Top. Catal. 11/12 (2000) 23.
[26] Y. Moro-oka, Appl. Catal. A 181 (1999) 323.
[27] J. Haber, Stud. Surf. Sci. Catal. 110 (1997) 1.
[28] G. Busca, E. Finocchio, V. Lorenzelli, G. Ramis, M. Baldi, Catal. Today 49 (1999) 453.
[29] M.Y. Sinev, J. Catal. 216 (2003) 468.
[30] S. Kuba, P.C. Heydorn, R.K. Grasselli, B.C. Gates, M. Che, H. Knözinger, Phys. Chem. Chem. Phys. 3 (2001) 146.
[31] G. Fu, X. Xu, X. Lu, H.L. Wan, J. Am. Chem. Soc. 127 (2005) 3989.
[32] G. Fu, X. Xu, X. Lu, H.L. Wan, J. Phys. Chem. B 109 (2005) 6416.
[33] Y.H. Jang, W.A. Goddard, J. Phys. Chem. B 106 (2002) 5997.
[34] E.F. Fialko, A.V. Kikhtenko, V.B. Goncharov, Organometalics 17 (1998) 25.
[35] D. Schroder, H.H. Schwarz, Angew. Chem., Int. Ed. Engl. 34 (1995) 1973.
[36] C.L. Hill, C.M. Prosser-McCartha, Coord. Chem. Rev. 143 (1995) 407.
[37] D.G. Barton, M. Shtein, R.D. Wilson, S.L. Soled, E. Iglesia, J. Phys. Chem. B 103 (1999) 630.
[38] K.D. Chen, A.T. Bell, E. Iglesia, J. Phys. Chem. B 104 (2000) 1292.
[39] S. Xie, K.D. Chen, A.T. Bell, E. Iglesia, J. Phys. Chem. B 104 (2000) 10059.
[40] W. Yang, X. Wang, Q. Guo, Q. Zhang, Y. Wang, New J. Chem. 27 (2003) 1301.
[41] A.D. Becke, Phys. Rev. A 38 (1988) 3098.
[42] C.T. Lee, W.T. Yang, R.G. Parr, Phys. Rev. B 37 (1988) 785.
[43] W.J. Hehre, R. Ditchfield, J.A. Pople, J. Chem. Phys. 56 (1972) 2257.
[44] P.C. Hariharan, J.A. Pople, Theo. Chim. Acta 28 (1973) 213.
[45] P.J. Hay, W.R. Wadt, J. Chem. Phys. 82 (1985) 299.
[46] M.J. Frisch, G.W. Trucks, H.B. Schlegel, G.E. Scuseria, M.A. Robb, J.R. Cheeseman, V.G. Zakrzewski, J.A. Montgomery Jr., R.E. Stratmann, J.C. Burant, S. Dapprich, J.M. Millam, A.D. Daniels, K.N. Kudin, M.C. Strain, O. Farkas, J. Tomasi, V. Barone, M. Cossi, R. Cammi, B. Mennucci, C. Pomelli, C. Adamo, S. Clifford, J. Ochterski, G.A. Petersson, P.Y. Ayala, Q. Cui, K. Morokuma, P. Salvador, J.J. Dannenberg, D.K. Malick, A.D. Rabuck, K. Raghavachari, J.B. Foresman, J. Cioslowski, J.V. Ortiz, A.G. Baboul, B.B. Stefanov, G. Liu, A. Liashenko, P. Piskorz, I. Komaromi, R. Gomperts, R.L. Martin, D.J. Fox, T. Keith, M.A. Al-Laham, C.Y. Peng, A. Nanayakkara, M. Challacombe, P.M.W. Gill, B. Johnson, W. Chen, M.W. Wong, J.L. Andres, C. Gonzalez, M. Head-Gordon, E.S. Replogle, J.A. Pople, Gaussian, Inc., Pittsburgh, PA, 2001.
[47] X. Xu, F. Faglioni, W.A. Goddard, J. Phys. Chem. A 106 (2002) 7171.
[48] A.K. Rappé, W.A. Goddard, Nature 285 (1980) 311.
[49] Unpublished result.
[50] K.D. Chen, A.T. Bell, E. Iglesia, J. Phys. Chem. B 104 (2000) 1292.
[51] At the same level of calculation, we find that the barrier for the most favorable H abstraction, from the central methylene C–H, is 43.5 kcal/mol, while the barrier for the most favorable (2 + 2), using the terminal methyl C–H, is 44.4 kcal/mol